



Q1 Diffusion tensor characteristics of gyrencephaly using high resolution diffusion MRI in vivo at 7T

Q2 Michiel Kleinnijenhuis ^{a,b,c*}, Tim van Mourik ^{a,1}, David G. Norris ^{a,d,e,1}, Dirk J. Ruiter ^{a,b,2},
4 Anne-Marie van Cappellen van Walsum ^{b,e,2}, Markus Barth ^{a,d,f,1}

⁵ ^a Radboud University Nijmegen, Donders Institute for Brain, Cognition and Behaviour, Centre for Cognitive Neuroimaging, Nijmegen, The Netherlands

⁶ ^b Radboudumc, Department of Anatomy, Nijmegen, The Netherlands

⁷ ^c University of Oxford, Oxford Centre for Functional MRI of the Brain, Oxford, UK

⁸ ^d Erwin L Hahn Institute for Magnetic Resonance Imaging, Essen, Germany

⁹ ^e University of Twente, MIRA Institute for Biomedical Technology and Technical Medicine, Enschede, The Netherlands

¹⁰ ^f The University of Queensland, Centre for Advanced Imaging, Brisbane, Australia

11 ARTICLE INFO

12 Article history:

13 Accepted 5 January 2015

14 Available online xxxx

A B S T R A C T

Gyration of the human cerebral cortex allows for the surface expansion that accommodates many more cortical neurons in comparison to other mammals. For neuroimaging, however, it forms a feature that complicates analysis. For example, it has long been established that cortical layers do not occupy the same depth in gyri and sulci. Recently, *in vivo* diffusion imaging has provided insights into the fibre architecture of the cortex, usually showing radial tensor orientations. This makes it relevant to investigate whether cortical diffusion tensor metrics depend on the gyral pattern. High-resolution (1 mm isotropic) diffusion weighted MRI of the medial wall of the hemispheres was performed at 7T. Diffusion data was resampled to surfaces in the cortex and underlying white matter, where the cortical surfaces obeyed the equivolume principle for cortical laminae over the cortical curvature. Diffusion tensor metrics were averaged over bins of curvature to obtain maps of characteristic patterns in the gyrus. Diffusivity, anisotropy and radially varied with curvature. Radiality was maximal in intermediate layers of the cortex next to the crown of the gyrus, not in white matter or on the crown. In the fundus, the deep cortical layers had tangential tensor orientations. In the white matter, tensor orientation changed from radial on the crown to tangential under the banks and fundus. White matter anisotropy gradually increased from the crown to the fundus. The characteristic pattern in the gyrus demonstrated here is in accordance with *ex vivo* diffusion MR microscopy and histological studies. The results indicate the necessity of taking into account the gyral pattern when cortical diffusion data is analysed. Additionally, the data suggest a confound for tractography approaches when reaching the gyrus, resulting in a possible bias towards the gyral crown. The implications for mechanisms that could drive cortical folding are discussed.

© 2015 Published by Elsevier Inc. 33

36

37 1. Introduction

38 Folding of the cerebral cortex is a distinct feature of the brain of
39 many mammals. Through the folding, the cortical sheet is curved in

convexities (gyri) and concavities (sulci). Gyrencephaly enables the cortical expansion that is particularly pronounced in humans. The mechanisms proposed for driving the folding can be divided in two categories: internal and external to the cortex. The differential expansion theory states that folding is internal to the cortex and occurs as a result of tangential expansion. A number of variants can be discerned, including differential growth of cortical layers (Richman et al., 1975), differential outgrowth of neurons from the subventricular zone (Kriegstein et al., 2006), and cytoarchitectural variance over regions (Ronan et al., 2013). The alternative hypothesis, put forward in Van Essen (1997), implicates folding to be driven by the external process of axonal tension. In Van Essen's tension-based morphogenesis model, cortical folding patterns are explained by mechanical forces in axons that pull densely connected areas (e.g. visual areas V1 and V2) together, resulting in compact wiring. Regardless of whether the curving cortex is a cause or effect, it is associated with two important neuroanatomical principles of gyrencephalic hemispheres: 1) geometric variations in

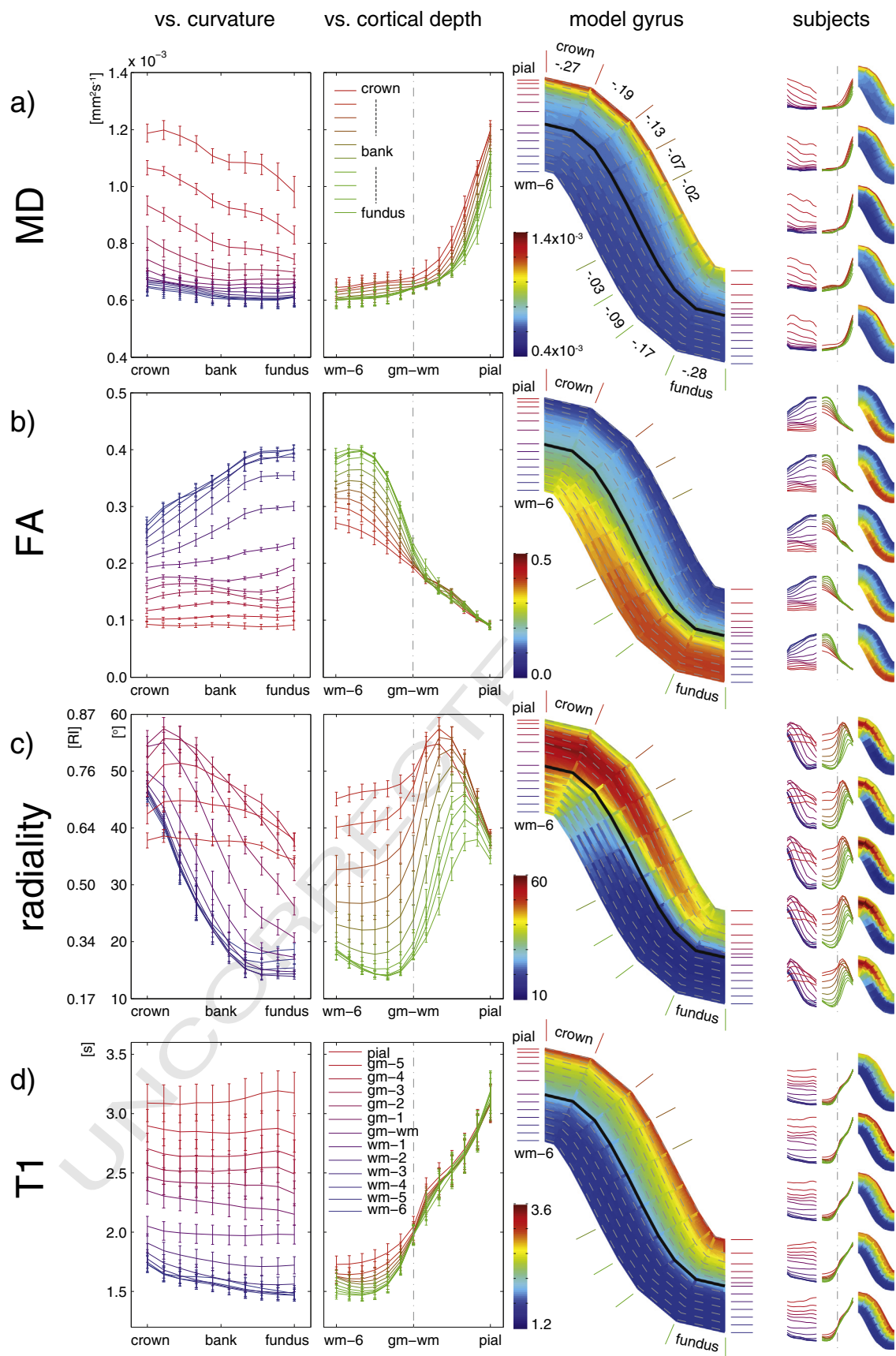
^{Abbreviations:} CSF, cerebrospinal fluid; DWI, diffusion weighted imaging; FA, fractional anisotropy; FOV, field of view; gm-x, grey matter surface no. x; GRE, gradient recalled echo; MD, mean diffusivity; MRI, magnetic resonance imaging; RI, radiality index; TA, acquisition time; TE, echo time; TI, inversion time; TR, repetition time; V1, primary visual cortex; V2, secondary visual cortex; WM-x, white matter surface no. x

* Corresponding author at: John Radcliffe Hospital, FMRI, Oxford OX3 9DU, United Kingdom.

E-mail addresses: michiel.kleinnijenhuis@ndcn.ox.ac.uk (M. Kleinnijenhuis), t.vanmourik@donders.ru.nl (T. van Mourik), d.norris@donders.ru.nl (D.G. Norris), Dirk.Ruiter@radboudumc.nl (D.J. Ruiter), Anne-Marie.vanCappellenvanWalsum@radboudumc.nl (A.-M.C. van Walsum), m.bARTH@uq.edu.au (M. Barth).

¹ Kappitelweg 29, Nijmegen, The Netherlands.

² Geert Grootplein Noord 21, Nijmegen, The Netherlands.



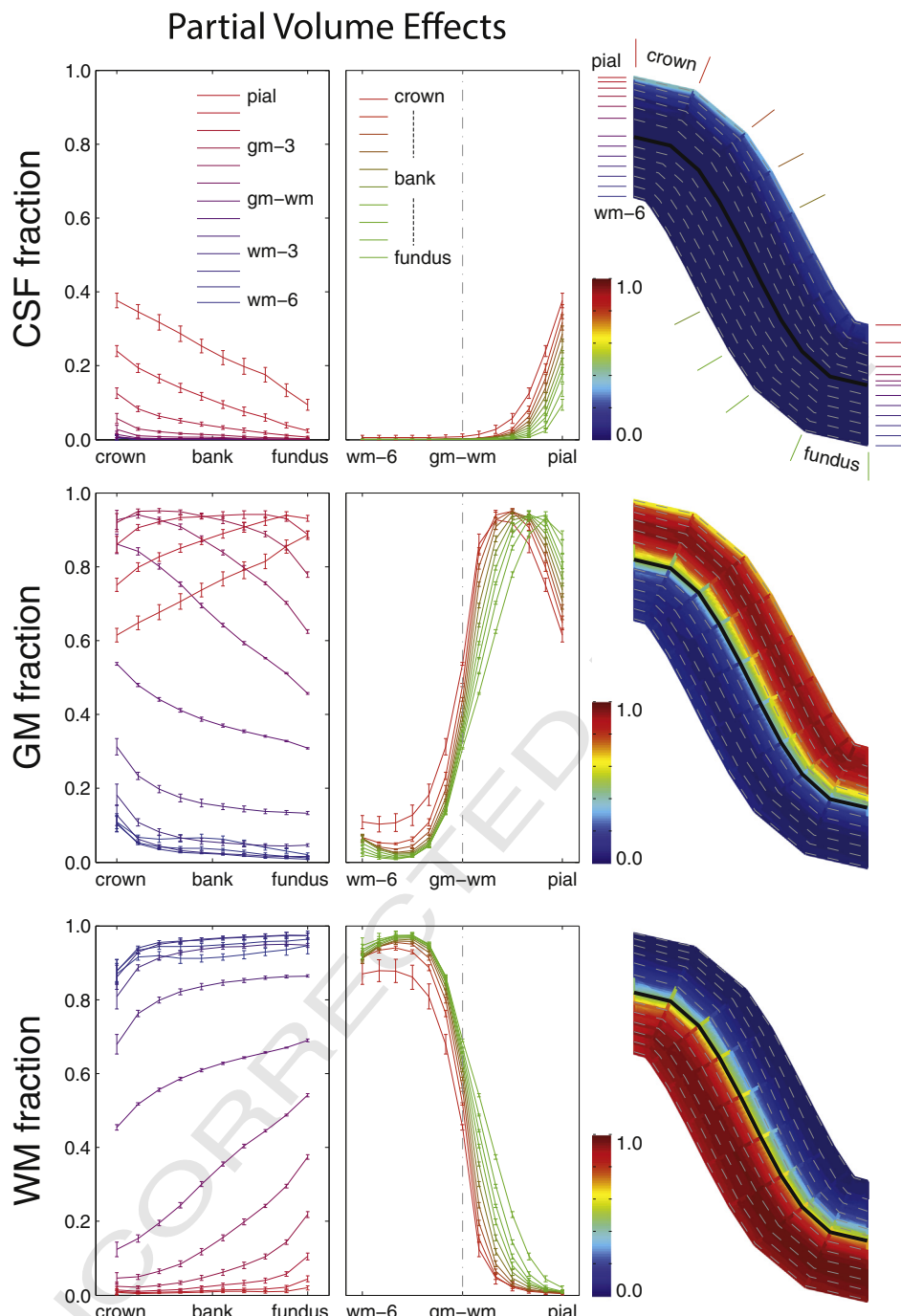


Fig. 2. Partial volume analysis. The fractions of CSF (top row), grey matter (middle row) and white matter (bottom row) are plotted against cortical curvature (left column) and surfaces (middle column). Colour-coded maps (right column) show the distribution of partial volume over the gyrus. The CSF has partial volume with grey matter in the superficial surfaces that is curvature dependent exhibiting higher partial volume on the crown. Also the partial volume of white and grey matter is dependent on the location on the cortical folds: for the deep surfaces in the fundus, the white matter fraction is higher as compared to the crown.

57 the laminar pattern of the neocortex, and 2) specific anatomy of fibres
58 in the gyrus.

59 As a cause or corollary of cortical curvature, the cytoarchitectonic
60 layers of the neocortex are a stack of curved sheets of which the surface

area varies in any folded cortical patch. *Id est*, the surface area of superficial layer I is larger than for deep layer VI on the crown of a gyrus, while it is smaller in the fundus of a sulcus. If homogeneity of functional anatomy, e.g. the distribution of minicolumns, is assumed over the cortical

Fig. 1. Model gyrus for the tensor metrics: a) mean diffusivity, b) fractional anisotropy, c) radially; and d) the T1 map. The graphs in the left column show the values over the ten cortical curvature bins for each surface (traces red to blue for pial surface to the depth of the white matter). The graphs in the second column show the orthogonal plot over the 13 cortical surfaces for each curvature bin (traces red to green for the crown to fundus). Error bars indicate standard deviation over subjects. The model gyrus represents the cortical depth and curvature dependence in colour-coded patches. The crown is on top, and the fundus on the bottom. The solid line in the middle represents the grey-white matter boundary; the grey dashed lines indicate the remaining surfaces. Note that the cortical surfaces are not equidistant. Numbers around the model in a) show curvature values for the curvature bins (bin 1 and 10 go to $-\infty$ and ∞ , respectively). The right column shows results (traces and patches) for the five individual subjects (scaling is identical to the average).

sheet (but within a certain cytoarchitectonic domain) it is expected that the number of neurons and associated neuropil – and hence the volume – is also constant over curvature for any particular layer. This equivolume principle implies that the thickness of the layers varies with curvature. In the context of the cortex, this was first proposed by Bok (1929) and recently revived for sampling cortical layers in modern MRI methods by Waechnert et al. (2013).

The connectivity perspective on cortical folding predicts the emergence of specific configurations of fibres around the cortex. These demand tools suitable for investigating how the fibre architecture relates to the cortical folds. In vivo investigation of fibres is arguably best performed with diffusion MRI. The limited resolution of the diffusion MRI technique has hitherto prohibited a thorough investigation of these fibres in the living human brain. Recently, improved methods have opened the opportunity to acquire high quality diffusion images at a resolution adequate for imaging fibres in and around the gyri of the cerebral hemispheres (Eichner et al., 2013; Frost et al., 2013; Heidemann et al., 2010; McNab et al., 2010). The fibres in the cerebral cortex can now be investigated in vivo. Regional variation has been shown in the orientation of the principal eigenvector of the cortical diffusion tensor in primary sensory vs. motor cortices (McNab et al., 2013). In that study, it was also noted that the precentral and postcentral gyral crowns are characterized by tensor radial to the cortical surface at the grey–white matter boundary, while the banks show a more tangential orientation. Similar patterns are evident in ex vivo MRI and histology of fibres in the gyrus.

In the present study, we investigate diffusion tensor metrics in and under the cortical sheet in relation to the cortical folding pattern. We use high-resolution in vivo diffusion MRI acquired at 7T to image the fibres of the cortex forming the medial wall of the hemispheres. Laminar analysis of the cortex and the underlying white matter is performed, observing the neuroanatomical principles of interaction between cortical lamination and folding by using an equivolume sampling method.

2. Methods

2.1. MR acquisition

MRI data was acquired from five healthy participants (3 male, 2 female) on a 7T MR system equipped with 70 mT/m gradients using 32-channel head coil (Siemens, Erlangen, Germany). The protocol included MP2RAGE and diffusion weighted imaging (DWI; 40 min). The MP2RAGE was acquired in sagittal slices at 0.75 mm isotropic resolution with scan parameters TR = 5000 ms; TE = 2 ms; TI1 = 900 ms; TI2 = 3200 ms; FOV = 225 × 240 mm; matrix = 300 × 320; 224 slices with 0.75 mm slice thickness; and TA = 13 min.

Diffusion images were acquired in sagittal orientation at 1 mm isotropic resolution in a slab centred on the interhemispheric fissure, thus covering the medial extent of each hemisphere. Because of specific absorption rate (SAR) constraints the number of slices varied between 32 and 42 for different subjects. Images were acquired with sixty-one diffusion gradient directions (b -value = 1000 s mm²: the maximum that still provided adequate signal for this resolution in a reasonable scan time at 7T) equally distributed over the sphere interleaved with seven non-diffusion-weighted images. For DWI, the RESOLVE sequence (Porter and Heidemann, 2009) was used with parameters TR = 5800 ms³; TE = 56 ms; 4 read-out segments; FOV 212 × 212 mm; matrix = 212 × 212; slice thickness = 1 mm; TA ≈ 40–45 min (depending on reacquisition of artefact-affected segments).

³ For one subject, TR was increased to 6500 ms to keep within SAR-limits, while retaining sufficient coverage.

2.2. Data analysis

To analyse the diffusion data in the cortical coordinate space, the boundaries of the cortex were reconstructed. FreeSurfer v5.1 (Dale et al., 1999; Fischl et al., 1999) was used to extract a mesh of the pial and white matter surface of the calculated T1-weighted image from the MP2RAGE scan. To use the full resolution of the MP2RAGE, the ‘noconform’ option was used in the FreeSurfer pipeline such that the data are not resampled to 1 mm isotropic voxel size. Also after brain mask segmentation on the original contrasts of the MP2RAGE, manual editing of the brainmask and white matter segmentations was required to obtain accurate surface reconstructions. Undersegmented areas at the pial surface and the bright arteries on the pial surface in the MP2RAGE’s calculated T1-weighted image were removed manually.

The diffusion volumes were realigned and corrected for non-linear distortion in the phase-encode direction using the Donders Diffusion toolbox (v2.9; running under Matlab 7.14 and SPM8). The non-diffusion weighted images were realigned (rigid body; normalized mutual information cost function) and averaged. This non-diffusion weighted average volume was coregistered (affine; normalized mutual information) to the T1 volume (brainmask) from the FreeSurfer reconstruction after which the unwarping procedure (Visser et al., 2012) refined the match to the T1-weighted image. The diffusion-weighted images were realigned (affine; normalized mutual information) to the average non-diffusion-weighted image. All DWI volumes were resampled by applying the concatenated affine and unwarping parameters.

To correct residual misalignment of the FreeSurfer surface meshes and the cortical boundaries in the DWI, a boundary registration was performed. The average of all diffusion-weighted images was used as a target volume. The approach is based on the algorithm by Greve and Fischl (2009). The registration algorithm minimizes a cost function that reflects the integral of the gradient calculated over 1/3 of the cortical depth (inwards and outwards) along the normal of the white matter surface. Examples of the results of the alignment procedures are available in Supplementary Fig. 1.

The T1 map (as derived from the MP2RAGE; Marques et al., 2010) and the diffusion-weighted images were resampled in cortical coordinate space. Only cortical vertices were entered in the analysis, excluding the vertices that close the gap that results from cutting the hemispheres and those outside the slab of the diffusion images (also for the T1 map). Thirteen surfaces were used insampling along the normal to the cortex Q3 from the pial surface across the grey–white boundary one cortical thickness into the white matter. In the white matter, six equidistant surfaces were used (excluding the white matter surface). Points of profiles that intersected the mesh (i.e. on the opposite side of a gyrus) were excluded from the analysis. In the cortex, five surfaces (additional to the white and pial surfaces) were calculated between the white and pial surface using equivolume sampling. This sampling method observes the anatomical principle that the volume ratio between the cortical layers is preserved over the gyral and sulcal pattern (Bok, 1929). It has previously been implemented for the level set analysis of MR images (Waechnert et al., 2013). In our approach, the sampling depth r is directly calculated from the cortical curvature (defined as the inverse of the radius R of the inscribed sphere) and thickness T at each vertex for each intermediate surface from the white matter surface for equivolume function $r(f)$. Here f indicates the volume fraction, being zero at the white matter surface and one at the pial surface ($0 \leq f \leq 1$)

$$r(f) = \sqrt[3]{((R+T)^3 - R^3)f + R^3}. \quad (1)$$

The derivation is given in Appendix A, as well as a figure showing a comparison between equidistant and equivolume sampling of the T1 map. The cortical thickness and curvature (average between white

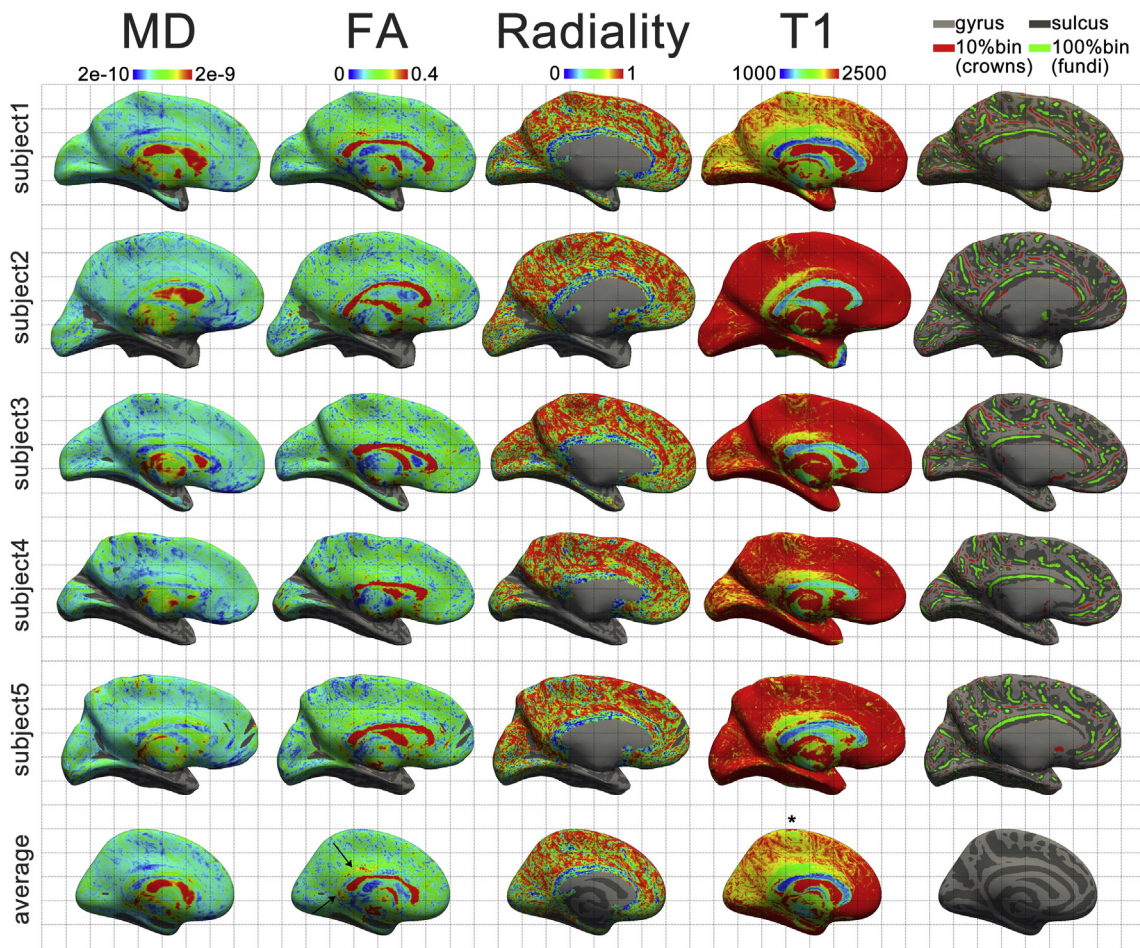


Fig. 3. Spatial maps of the medial wall of the left hemisphere for grey matter surface gm-3 (surface at 50% cortical volume). Rows show different subjects and the average over subjects projected onto FreeSurfer's fsaverage. Columns from left to right: the mean diffusivity (MD in $10^6 \text{ mm}^2 \text{ s}^{-1}$), the fractional anisotropy (FA), the radiality index, the T_1 map (in ms) and the gyral/sulcal pattern showing the locations of the 10th (crowns, red) and 100th (fundi, green) percentile curvature bins. The equivalent images for surfaces [wm-6, wm-3, gm-wm, gm-3, pial] can be found online as Supplementary Figure S3-7 (i.e. it also includes the present figure for completeness).

and pial curvature) were taken from the FreeSurfer output, where their computation is part of the standard pipeline.

Following McNab et al. (2013), the sampled surfaces are referred to as *surfaces*, not layers. This is to avoid confusion with histological layers. While the equivolume approach is in principle able to sample the histological layers by choosing the appropriate equivolume function, the present work uses a linear equivolume function with six steps for sampling grey matter surfaces. Surfaces are counted from the grey-white matter boundary, thus from pial to the deepest white matter surface the surfaces are referred to as: [pial, gm-5, gm-4, gm-3, gm-2, gm-1, gm-wm, wm-1, wm-2, wm-3, wm-4, wm-5, wm-6].

To assess the effects of partial volume between cerebrospinal fluid, cortex and white matter the method in Polimeni et al. (2010) was used. Briefly, high resolution masks of CSF, cortex and white matter were created (0.25 mm isotropic resolution) by filling the space outside the pial surface mesh, the space in between the pial and white surface and inside the white surface, respectively. These masks were linearly interpolated to the diffusion voxel grid to yield maps that approximate the contribution of the three tissue types to each voxel.

The diffusion tensor, its eigenvalues and eigenvectors and its derived metrics (mean diffusivity MD, fractional anisotropy FA) were calculated for each vertex with the Camino Diffusion MRI toolkit (Cook et al., 2006) v1011. To quantify tensor orientation with respect to the cortical coordinate frame, the angle between the cortical surface and the first eigenvector of the diffusion tensor was determined. Additionally, the radiality index (McNab et al., 2013) was calculated by taking the absolute value

of the dot product between the cortex normal \hat{v}_N and the primary eigen- 209 vector of the diffusion tensor \hat{e}_1 : 210

$$\text{radiality} = |\hat{v}_N \cdot \hat{e}_1|. \quad (2) \quad 212$$

To assess the variation of the computed measures with cortical curvature, the vertices were stratified in ten bins spanning the 10th, 213 20th, ..., 100th percentiles of the cortical curvature concatenated over 214 both hemispheres of all subjects. Measures were averaged over these 215 bins and visualized on a model of a gyrus. Also, mean and standard 216 deviations over subjects were computed and the mean was plotted on 217 the same model gyrus. The same procedure was applied to the partial 218 volume maps. 219

Using FreeSurfer, average spatial maps were computed over subjects 220 by first transforming the vertices of each subject to the 'fsaverage' 221 subject. For the diffusion measures, only vertices for which data was 222 available for all subjects were included. The subject-specific and average 223 spatial maps were visualized in FreeView. 224

2.3. Results

Diffusion tensor metrics exhibited a dependence on cortical curva- 226 ture as well as on cortical depth. This is visualized in Fig. 1 showing a 227 model gyrus from crown to fundus including surfaces in the white and 228 grey matter on which diffusion tensor metrics are projected. In Supple- 229 mentary Fig. 2, histograms show the distributions of the metrics. 230

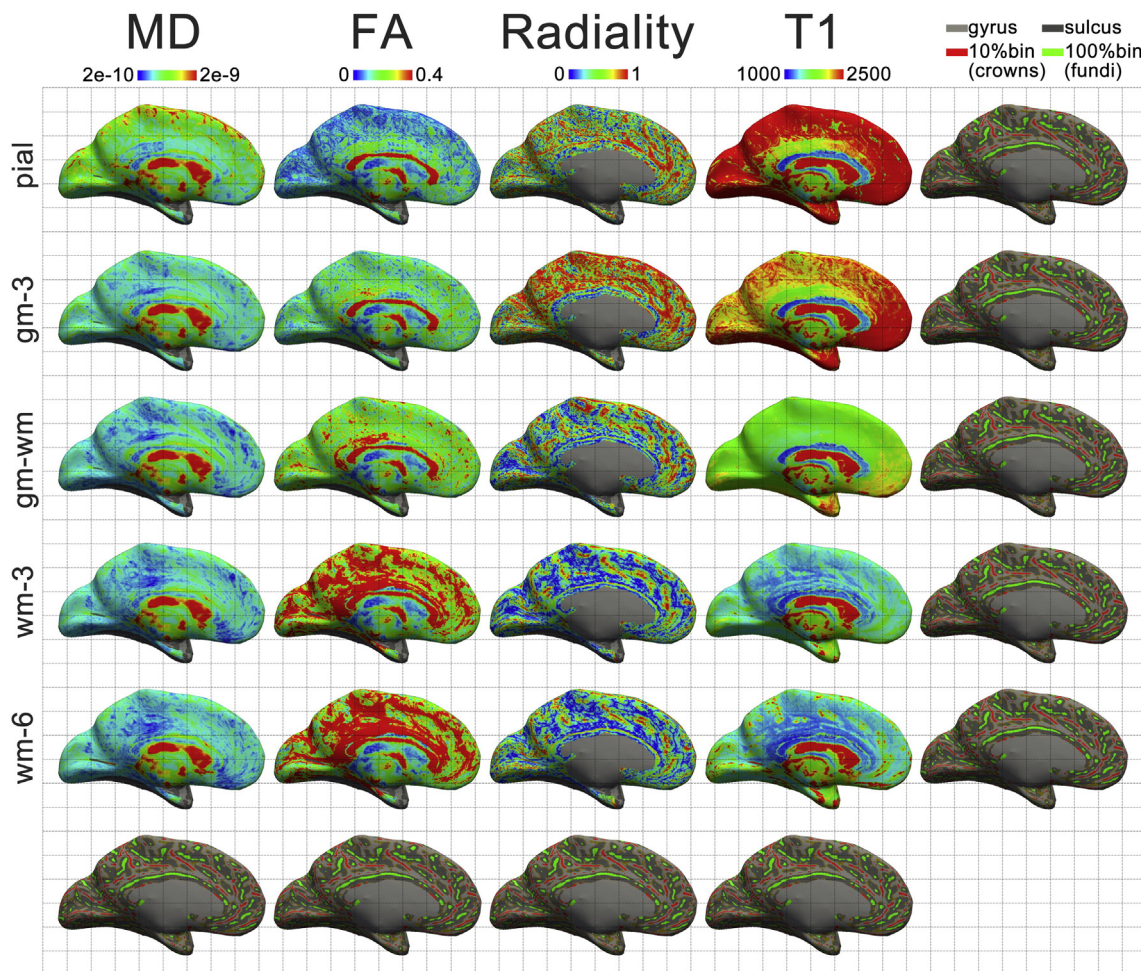


Fig. 4. Spatial maps of the medial wall of the left hemisphere for subject 1 for surfaces [pial, gm-3, gm-wm, wm-3, wm-6] in the different rows. Columns from left to right: the mean diffusivity (MD in $10^6 \text{ mm}^2 \text{ s}^{-1}$), the fractional anisotropy (FA), the radiality, the T1 map (in ms) and the gyral/sulcal pattern showing the locations of the 10th (crown, red) and 100th (fundus, green) percentile curvature bins (repeated in the last row to facilitate identifying gyri/sulci). The maps of other subjects are available as Supplementary Figure S8–12 and the average as Supplementary Figure S13.

231 The mean diffusivity (MD, Fig. 1a) map was high for the most super-
232 ficial surface and declined towards the white matter. MD is lower in the
233 fundus compared to the crown for any given surface; a feature that is

most pronounced for the most superficial grey matter surfaces (gm-4, 234
gm-5, pial). MD of the superficial surfaces appears to follow the CSF 235
partial volume map (Fig. 2; first row) 236

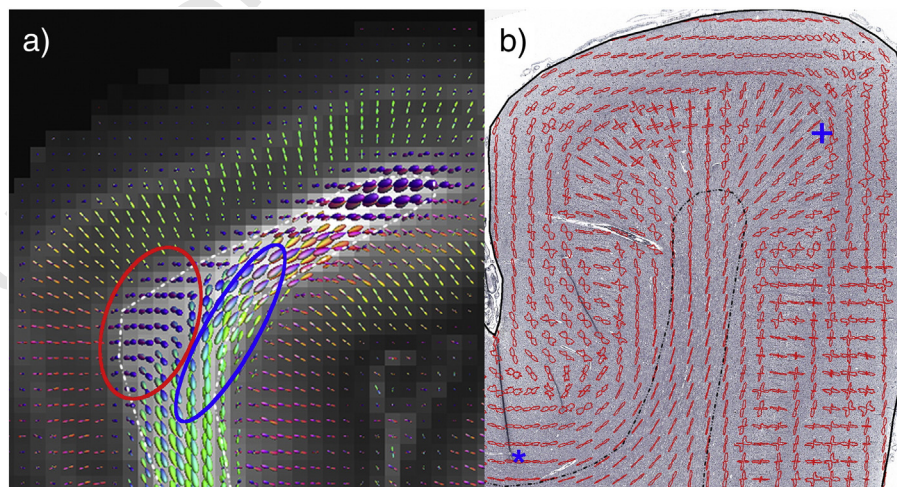


Fig. 5. MR and light microscopy of fibres in the gyrus. a) fibre orientation distribution functions derived from ex vivo MR diffusion microscopy of the primary visual cortex. U-fibres in the concavity of the cortical fold are in the in-plane direction over the gyrus (right ellipse), while u-fibres in the convexity are mostly directed along the length of the gyrus. The approximate grey-white matter boundary is drawn as a dashed line. Radial fibres are found throughout the infragranular layers of the cortex. b) histological fibre orientation distribution from the primary visual cortex overlaid on the Bodian-stained section. Asterisk (*) indicates dominant tangential orientation of the infragranular layers in the fundus of the sulcus. Plus (+) shows the region of maximal radiality (note: away from the gyral crown). Adapted from Kleinnijenhuis et al. (2013).

237 The fractional anisotropy (FA, Fig. 1b) differs between grey and
 238 white matter, but also shows variation with cortical curvature. In the
 239 white matter, FA is the highest under the fundus tapering off towards
 240 the crown. The curvature dependence is reversed in the middle cortical
 241 surfaces (gm-2, gm-3, gm-4), where FA is relatively high on the crown,
 242 but low in the fundus. The top two grey matter surfaces have a consis-
 243 tently low anisotropy over the gyral/sulcal pattern, while the anisotropy
 244 at the grey–white matter boundary is intermediate between white and
 245 grey and shows a small linear increase towards the fundus. This is
 246 consistent with a decrease in the grey matter fraction in the partial
 247 volume maps from crown to fundus.

248 The radiality reflects the orientation of the tensor with respect to the
 249 cortical sheet (Fig. 1c). It features a marked gyral/sulcal pattern for grey
 250 as well as white matter and a laminar pattern in the cortex. Radiality is
 251 maximal in the second curvature bin near (but not on) the crown in the
 252 second grey matter surface (gm-2). Towards the fundus, the peak
 253 radiality within the curvature bins becomes more superficial, similar
 254 to the grey matter fraction in the partial volume map (Fig. 2, middle
 255 row). Towards the fundus, radiality decreases for all surfaces within
 256 the cortex. The decrease is gradual for the surfaces near the pial surface
 257 (gm-4, gm-5) and sharp for the surfaces near the gm-wm boundary.
 258 The radiality on the pial surface is intermediate (or almost random)
 259 for all curvature bins. On the grey–white matter boundary (gm-wm),
 260 the tensor orientation is similar to that in the WM. Under the fundus,
 261 tensors are predominantly oriented tangential to the cortical sheet.
 262 Moving towards the crown through the white matter, there is a steep,
 263 but gradual increase in radiality from the bank of the sulcus to the
 264 crown. The average radiality of the tensors under the crown is lower
 265 as compared to the radiality of the cortical tensors in the crown.

266 The T1 map was also projected on the model gyrus (Fig. 1d). It shows
 267 a general similarity to the MD map. No curvature dependence was
 268 observed for the T1 map.

269 The spatial maps of the cortical tensor metrics at the intermediate
 270 surface (gm-3) of the hemispheres' medial walls are shown in Fig. 3.
 271 Alongside, the gyral/sulcal pattern and the T1 map are incorporated.
 272 The maps show curvature-dependent variations for all measures, par-
 273 ticularly for radiality. The radiality index (third column) approaches
 274 its maximum value (i.e. 1) for a substantial area of the cortex (red), ex-
 275 cept the fundi (green). Tensors in the callosal sulcus are consistently
 276 tangential (blue ring around corpus callosum). The FA and T1 maps
 277 show peaks in the posterior cingulate gyrus and isthmus of the cingulate
 278 gyrus (black arrows; third column, bottom row). The FA and T1 maps
 279 are also highly similar for surfaces sampled in the white matter (Supple-
 280 mentary Figure S3–7 for wm-6, wm-3, gm-wm, gm-3 and pial). In the
 281 T1 map, a minimum is seen for the primary areas of the paracentral
 282 lobule (black asterisk in bottom row).

283 The variation of the spatial maps over cortical depth is shown in
 284 Fig. 3. Mean diffusivity is increased over the entire cortical sheet on
 285 the pial surface (first row) compared to the deeper grey and white mat-
 286 ter surfaces. Fractional anisotropy is low on the pial surface and radiality
 287 appears random. In the cortex (second row), FA increases independent
 288 of the gyral/sulcal pattern. The radiality shows distinct correlation with
 289 the gyral pattern here, where fibres are predominantly radial on the
 290 crown and banks (red, fourth column, second row), but more tangential
 291 in the fundi. In the white matter, the radiality on the banks reverses to
 292 tangential (blue, third column, fourth and fifth row). While the FA is
 293 fairly homogeneous at the grey–white matter boundary, the FA map
 294 shows pronounced minima under the crowns sampling into the white
 295 matter (green, third column, fourth and fifth row).

296 2.4. Discussion

297 The fibre anatomy in and around the neocortex is highly dependent
 298 on the cortical curvature. This has been acknowledged by early investi-
 299 gators such as Theodor Meynert, who was the first to cytoarchitecturally
 300 classify the cortical layers and describe the u-shaped short range

301 association fibres that line the folds of the cortical sheet using post-
 302 mortem histology (Meynert, 1885). In the present study, we have
 303 shown that the curvature-dependence of these fibres can be investigat-
 304 ed with *in vivo* MRI methodology. We have observed variations in
 305 radiality and anisotropy between gyral crowns and sulcal fundi as well
 306 as depth-dependent effects on these measures (Fig. 5). Q4

307 The radiality and anisotropy variations with curvature are in accor-
 308 dance with previous *ex vivo* MR microscopy and histological investiga-
 309 tions. The laminar profile of the orientation of diffusion tensors (and
 310 other diffusion models) has been investigated in detail for the primary
 311 visual cortex (Kleinnijenhuis et al., 2012; Leuze et al., 2012) showing
 312 pronounced radiality above and below the granular layer. Furthermore,
 313 these investigations show the least tangential components in the fibre
 314 orientation distributions over the gyral crown, which was reflected in
 315 the maximum for radiality in the gyral crown *in vivo*. 315

316 The average peak radiality did not occur in the white matter under
 317 the crown, but in the grey matter of the cortex. One possible explanation
 318 is that, next to fibres that project into the crown radially, there is a
 319 second fibre component under the crown that reduces tensor radiality.
 320 This second component might be formed by u-fibres. Putatively, these
 321 fibres course tangential to the cortical sheet over the length of a gyrus,
 322 whereas sulcal u-fibres often course in a direction perpendicular to a
 323 gyrus. Both types are shown in Fig. 4a that shows fibre orientation
 324 distributions from *ex vivo* diffusion MR microscopy and histology. Alter-
 325 natively, the reduced average radiality under the crown could also
 326 reflect regional variation in the fibre configurations under the crown.
 327 In most regions, fibres may project radially into the crown, while in
 328 other regions fibre bundle may course tangentially along the gyrus.
 329 For example, the cingulum, which constitutes a large area of the cortex
 330 investigated in the present study, courses through the cingulate gyrus
 331 tangential to the cortical sheet. 331

332 The peak radiality shifted from deeper to more superficial surfaces
 333 from crown to fundus. As a similar shift was observed for the grey mat-
 334 ter fraction it seems more likely that this effect is a result of partial
 335 volume effects as opposed to a difference in the fibre coherence within
 336 histological layers between crowns and fundi. The radiality at the pial
 337 surface was intermediate and relatively stable over the curvature
 338 pattern. This suggests isotropic diffusion with an almost random ori-
 339 entation of the tensor. This is likely due to partial volume with CSF. An
 340 alternative explanation might be that tangential (Leuze et al., 2012) as
 341 well as radial fibre components are present in upper layers of the cortex. 341

342 The infragranular layers of the fundus showed tensors oriented
 343 tangential to the cortical sheet. Tangential fibre orientation distributions
 344 in the infragranular fundus can also be observed in Fig. 4, for both
 345 *ex vivo* MR microscopy and histology (see also Budde and Annese,
 346 2013; Kleinnijenhuis et al., 2013). The cortical fibres run in parallel
 347 with the u-fibre bundle, but it is unclear from these data where the
 348 fibre project. First, the fibres could end in the fundus, which has the
 349 implication that – unlike on the crown – the cortical projection has a
 350 preferential tangential approach. This might seem counterintuitive for
 351 fibres projecting from the deep white matter. However, it is not unlikely
 352 that local corticocortical projections dominate the radially oriented
 353 deep white matter fibres entering the cortex. Second, the tangential fi-
 354 bres of the lower layers of the fundus could be u-fibres that mix with
 355 the fibres of the lower layer of the cortex. This distinct mixing in the
 356 fundus might be a consequence of tension building in the fibres during
 357 the developmental stage in which cortical folding occurs. In that case, it
 358 is likely that the tension results from the sulcus deepening over time,
 359 stretching the u-fibre bundles over fundi, potentially also increasing
 360 the axon packing density and therefore leading to the high FA observed
 361 in these u-fibre bundles. Tension in the white matter under the fundus
 362 is predicted by the finite element model for differential cortical expan-
 363 sion of the form presented by Xu et al. (2010). The alternative axonal
 364 tension hypothesis (Van Essen, 1997) predicts the u-fibres over the
 365 fundus to be 'weak' connections, while those connecting opposing
 366 banks are predicted to be 'strong'. Our *ex vivo* MR microscopy and 366

histological data do not indicate any strong projection connecting opposing banks of a gyrus, as was also pointed out in Ronan et al. (2013). If we may abuse FA as measure of the strength of a projection, the stronger projection surely seems to be over the fundus, as seen in vivo and ex vivo MRI. However, it cannot be precluded that the primary mechanism for folding is axonal tension. It should be kept in mind that the density of a projection in *development* would be decisive for the folding behaviour, not that observed in adulthood. Furthermore, the projection density over the fundus may only appear to be denser than between opposing banks, simply for the reason that fibres between the banks are likely to be distributed over the gyrus, while fibres destined for the neighbouring bank all aggregate into the u-fibre having a much smaller cross-sectional area.

The hypothesis that the crowns of the gyri are the primary axon termination areas – as has been inferred from tractography (Nie et al., 2012) – is easily explained by the canonical gyral fibre layout demonstrated in the present study. Because the FA is high and fibres are tangential under the fundus, it is less likely for tractography to reach a stopping criterion. Rather, streamlines approaching the fundus would join the u-fibre and continue to the gyral crown. This presents a confound for the axonal pushing theory (Chen et al., 2013; Nie et al., 2012) of cortical folding that has been based on the tractography results. Moreover, it implies a serious confound for tractography in general.

FA and T1 show curvature-dependent variation over cortical depth. The equivolume-sampled values for the different surfaces, however, are relatively stable over the gyral–sulcal pattern. This suggests that these values are homogeneous within cortical layers. Therefore, the curvature dependence is likely to be an artefact of the volume preserving principle, i.e. the laminae characterized by low FA/high T1 occupy a larger fraction of the cortical thickness in the fundus than on the crown. Contrary to what was found by other investigators (Sereno et al., 2013), and assuming equivolume-sampling is anatomically correct, T1 does not appear to vary with cortical curvature in our data. FA does show a slight residual variation for the intermediate cortical layers, indicating FA is lower in the fundus as compared to the crown. With regard to the underlying anatomy, the radiality provides a clue: it appears that the low FA values in the deep grey matter surfaces (gm-2, gm-3) of the fundus overlap with a change from radial to tangential fibre configurations, i.e. a region where both configurations occur equally.

The in vivo diffusion data was limited to 1 mm isotropic voxels. Although this is already a tremendous improvement over the typical 2 mm isotropic resolution, it may still be insufficient to sample the layers of the cortex. Because the voxel matrix is oriented arbitrarily with respect to the orientation of the folded cortical sheet, however, the cortical layers overlap with the voxel centres equally often and averaging over all profiles in the curvature bins results in smooth cortical profiles (see Koopmans et al. (2011) for a thorough discussion of the effective resolution of cortical sampling). As illustrated by the partial volume analysis, the laminar results should nevertheless be interpreted with care, heeding the possibility that some results could be due to partial volume with either cerebrospinal fluid in the supragranular layers, or with the white matter in the infragranular layers. The laminar variation in the mean diffusivity, for example, is likely to be due to partial volume with CSF (that has a very high diffusivity). However, a small difference might exist in the MD for supragranular vs. infragranular layers, as has previously been found ex vivo (Kleinnijenhuis et al., 2013).

As shown in the current study, the partial volume effect also varies with the curvature of the cortex. CSF has the largest impact on the cortical signal on the crown, while white matter partial volume is prominent in the fundus. This has two reasons. First, the CSF in between the folds of the cortex only occupies the narrow space between the folds, while on the crowns larger CSF-filled spaces line the cortex. This might, for example, explain the sharper decrease of MD from crown to bank as compared to the decrease from bank to fundus in the superficial surfaces of the cortex. Second, the equivolume sampling approach samples surfaces that are more closely spaced and near the CSF for the

crown, while more closely spaced near the white matter at the fundus. Thus, although the PVE is geometrically homogeneous, our inhomogeneous anatomical sampling introduces variance in the relative partial volume over the sampled surface.

Because of constraints in power deposition, the diffusion acquisition was limited to the medial wall of the hemisphere. Therefore, bias might exist in the results towards fibre configurations dominant in these areas. In general, this raises the question about variability in cortical fibre configurations over regions, as has been demonstrated for primary motor vs. primary sensory cortex (McNab et al., 2013). One might speculate on the usefulness for segmentation of the cortical sheet. Indeed, a feature vector representation of the cortical diffusion signal has been used for successful and reproducible identification of particular visual areas such as area MT+ and the angular gyrus (Nagy et al., 2013). To further develop these methods, high spatial and angular resolution diffusion data, as well as multiple *b*-values are expected to contribute to the application of better models for this purpose. Obtaining such datasets in reasonable time in vivo could soon be possible with multi-band diffusion acquisition (Eichner et al., 2013; Frost et al., 2013).

Supplementary data to this article can be found online at <http://dx.doi.org/10.1016/j.neuroimage.2015.01.001>.

Acknowledgments

The authors acknowledge the contributions to this research of Lena Schäfer for help with data acquisition, Emil Nijhuis and Saad Jbabdi for advice on data analysis and Siemens (Erlangen, Germany) for providing the RESOLVE WIP package. The research was funded by Ministerie van Economische Zaken, Provincie Overijssel and Provincie Gelderland through the ViP-BrainNetworks project. The funding bodies had no involvement in the preparation of the manuscript.

Appendix A. Equivolume surfaces

The equivolume principle states that the cortical layers within an area preserve the volume ratio, in straight pieces of cortex, as well as in gyri and sulci. This ratio is linked to the curvature and thickness of the cortex at a given point.

Consider two concentric spheres (Fig. A1), the first one smaller than the second. The first has radius R , the second has radius $R + T$, with $T > 0$.

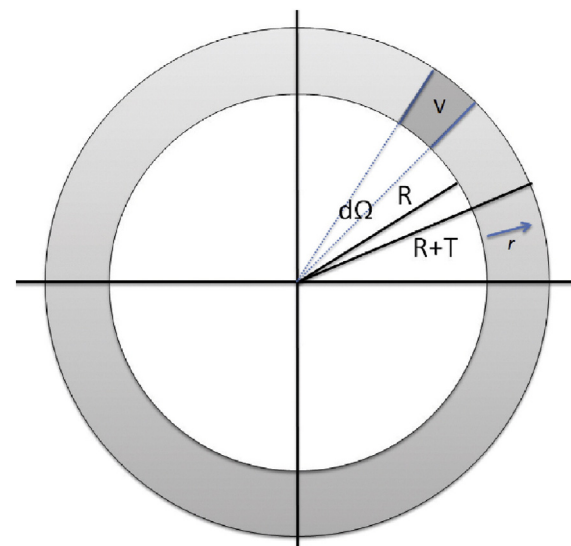


Fig. A1. Cross-section of concentric spheres illustrating calculation of cortical depth given a volume fraction, cortical thickness and curvature.

470 The total volume between the spheres for a differential solid angle
471 $d\Omega$ is given by

$$473 V_{total} = \int_{r=R}^{r=R+T} r^2 dr d\Omega \quad (3)$$

$$474 V_{total} = \left[\frac{1}{3} r^3 \right]_{r=R}^{r=R+T} d\Omega \quad (4)$$

$$475 V_{total} = \frac{1}{3} ((R+T)^3 - R^3) d\Omega. \quad (5)$$

476 Now we are interested in obtaining the radius r corresponding to
477 some fraction f of the total volume V_{total} . We create a volume fraction
478 function $f(r)$ that runs from R to $R + T$ and has to satisfy $f(R) = 0$ and
479 $f(R + T) = 1$.

480 The volume from the inner radius R to some radius r is given by

$$481 V(r) = \int_{r'=R}^{r'=r} r'^2 dr' d\Omega \quad (6)$$

$$482 V(r) = \left[\frac{1}{3} r'^3 \right]_{r'=R}^{r'=r} d\Omega \quad (7)$$

$$483 V(r) = \frac{1}{3} (r^3 - R^3) d\Omega. \quad (8)$$

484 Thus, the volume fraction function is simply given by

$$485 f(r) = \frac{V(r)}{V_{total}} \quad (9)$$

$$486 f(r) = \frac{\frac{1}{3} (r^3 - R^3) d\Omega}{\frac{1}{3} ((R+T)^3 - R^3) d\Omega} \quad (10)$$

$$487 f(r) = \frac{r^3 - R^3}{(R+T)^3 - R^3}. \quad (11)$$

488 Generally, we are interested in r as a function of f , and hence
489 rearranging the equation in this form gives:

$$490 r(f)^3 = ((R+T)^3 - R^3)f + R^3. \quad (12)$$

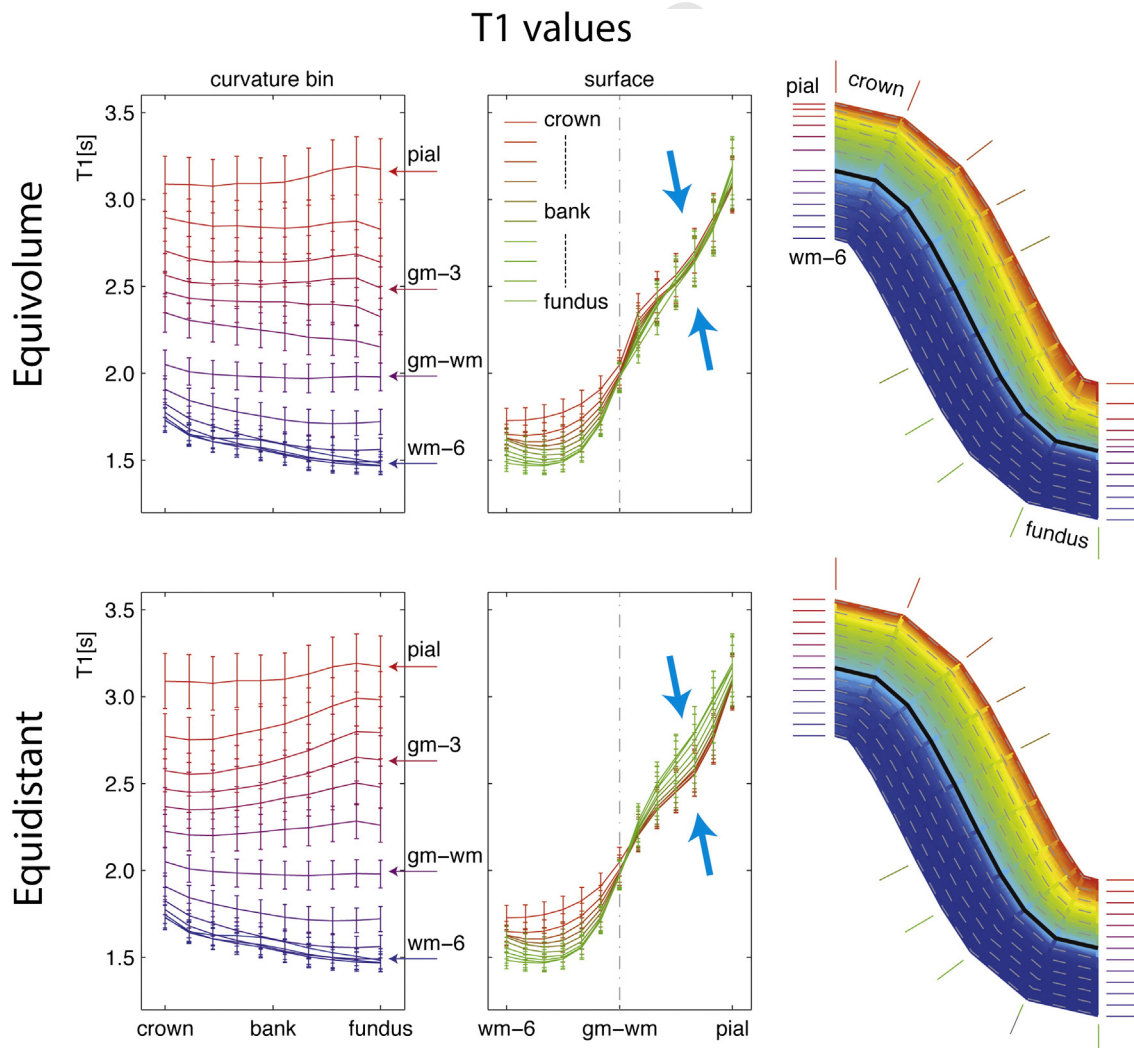


Fig. A2. Comparison of profiles of T1 values with equivolume sampling (top row) and equidistant sampling (bottom row).

Taking the cube root of both sides gives a direct formula for r :

$$r(f) = \sqrt[3]{((R + T)^3 - R^3)f + R^3} \quad (13)$$

The putative increase in accuracy associated with this sampling approach is demonstrated in Fig. A2. If it is assumed that T1 values are homogeneous within histological layers over the cortical sheet the plots of T1 vs. curvature should be flat within the cortex (first column) and the plots of T1 vs. cortical depth for different curvature bins should overlap (middle column, blue arrows). With the equidistant sampling, a dependence of T1 on cortical curvature is seen, as judged from the slope of the lines in the first column and diverging traces in the middle column. With equivolume sampling, however, flat lines and a much better overlap are observed. From equidistantly sampled surfaces we might have reason to believe that T1 values are not homogeneous within layers over the cortical sheet, while the equivolume sampling suggests that cortical T1 actually does not depend on the folding pattern.

References

- Bok, S., 1929. Der Einfluß der in den Furchen und Windungen auftretenden Krümmungen der Großhirnrinde auf die Rindenarchitektur. *Z. Gesamte Neurol. Psychiatr.* 12, 682–750.
- Budde, M.D., Annese, J., 2013. Quantification of anisotropy and fiber orientation in human brain histological sections. *Front. Integr. Neurosci.* 7, 1–8. <http://dx.doi.org/10.3389/fint.2013.00003> (February).
- Chen, H., Zhang, T., Guo, L., Li, K., Yu, X., Li, L., Liu, T., 2013. Coevolution of gyral folding and structural connection patterns in primate brains. *Cereb. Cortex* 23 (5), 1208–1217. <http://dx.doi.org/10.1093/cercor/bhs113> (New York, N.Y.: 1991).
- Cook, P.A., Bai, Y., Seunarine, K.K., Hall, M.G., Parker, G.J., Alexander, D.C., 2006. Camino: open-source diffusion-MRI reconstruction and processing. Proceedings of the International Society for Magnetic Resonance in Medicine. vol. 14, p. 2759 (Seattle, WA, USA).
- Dale, A.M., Fischl, B., Sereno, M.I., 1999. Cortical surface-based analysis. I. Segmentation and surface reconstruction. *NeuroImage* 9 (2), 179–194. <http://dx.doi.org/10.1006/nimg.1998.0395>.
- Eichner, C., Setsompop, K., Koopmans, P.J., Lützkendorf, R., Norris, D.G., Turner, R., Heidemann, R.M., 2013. Slice accelerated diffusion-weighted imaging at ultra-high field strength. *Magn. Reson. Med.* <http://dx.doi.org/10.1002/mrm.24809>.
- Fischl, B., Sereno, M.I., Dale, A.M., 1999. Cortical surface-based analysis. II: Inflation, flattening, and a surface-based coordinate system. *NeuroImage* 9 (2), 195–207. <http://dx.doi.org/10.1006/nimg.1998.0396>.
- Frost, R., Miller, K.L., Tijssen, R.H.N., Porter, D.A., Jezzard, P., 2013. 3D Multi-slab diffusion-weighted readout-segmented EPI with real-time cardiac-reordered k-space acquisition. *Magn. Reson. Med.* <http://dx.doi.org/10.1002/mrm.25062>.
- Greve, D.N., Fischl, B., 2009. Accurate and robust brain image alignment using boundary-based registration. *NeuroImage* 48 (1), 63–72. <http://dx.doi.org/10.1016/j.neuroimage.2009.06.060>.
- Heidemann, R.M., Porter, D.A., Anwander, A., Feiweier, T., Heberlein, K., Knösche, T.R., Turner, R., 2010. Diffusion imaging in humans at 7T using readout-segmented EPI and GRAPPA. *Magn. Reson. Med.* 64 (1), 9–14. <http://dx.doi.org/10.1002/mrm.22480>.
- Kleinnijenhuis, M., Zerbi, V., Küsters, B., Slump, C.H., Barth, M., van Cappellen van Walsum, A.-M., 2012. Layer-specific diffusion weighted imaging in human primary visual cortex in vitro. *Cortex* 1–14 <http://dx.doi.org/10.1016/j.cortex.2012.11.015>.
- Kleinnijenhuis, M., Zhang, H., Wiedermann, D., Küsters, B., Norris, D.G., van Cappellen van Walsum, A.-M., 2013. Detailed laminar characteristics of the human neocortex revealed by NODDI and histology. *Human Brain Mapping*, p. 3815 (Seattle, WA, USA).
- Koopmans, P.J., Barth, M., Orzada, S., Norris, D.G., 2011. Multi-echo fMRI of the cortical laminae in humans at 7T. *NeuroImage* 56 (3), 1276–1285. <http://dx.doi.org/10.1016/j.neuroimage.2011.02.042>.
- Kriegstein, A., Noctor, S., Martínez-Cerdeño, V., 2006. Patterns of neural stem and progenitor cell division may underlie evolutionary cortical expansion. *Nature Reviews. Neuroscience* 7 (11), 883–890. <http://dx.doi.org/10.1038/nrn2008>.
- Leuze, C.W.U., Anwander, A., Bazin, P.-L., Dhital, B., Stüber, C., Reimann, K., Turner, R., 2012. Layer-specific intracortical connectivity revealed with diffusion MRI. *Cereb. Cortex* <http://dx.doi.org/10.1093/cercor/bhs311> (New York, N.Y.: 1991).
- Marques, J.P., Kober, T., Krueger, G., van der Zwaag, W., Van de Moortele, P.-F., Gruetter, R., 2010. MP2RAGE, a self bias-field corrected sequence for improved segmentation and T1-mapping at high field. *NeuroImage* 49 (2), 1271–1281. <http://dx.doi.org/10.1016/j.neuroimage.2009.10.002>.
- McNab, J.A., Gallichan, D., Miller, K.L., 2010. 3D steady-state diffusion-weighted imaging with trajectory using radially batched internal navigator echoes (TURBINE). *Magn. Reson. Med.* 63 (1), 235–242. <http://dx.doi.org/10.1002/mrm.22183>.
- McNab, J.A., Polimeni, J.R., Wang, R., Augustinack, J.C., Fujimoto, K., Stevens, A., Wald, LL., 2013. Surface based analysis of diffusion orientation for identifying architectonic domains in the in vivo human cortex. *NeuroImage* 69, 87–100. <http://dx.doi.org/10.1016/j.neuroimage.2012.11.065>.
- Meynert, T., 1885. A Clinical Treatise on Diseases of the Fore-brain Based upon a Study of its Structure, Functions, and Nutrition. Translated by Bernard Sachs. G.P. Putnam's Sons, New York.
- Nagy, Z., Alexander, D.C., Thomas, D.L., Weiskopf, N., Sereno, M.I., 2013. Using high angular resolution diffusion imaging data to discriminate cortical regions. *PLoS ONE* 8 (5), e63842. <http://dx.doi.org/10.1371/journal.pone.0063842>.
- Nie, J., Guo, L., Li, K., Wang, Y., Chen, G., Li, L., Liu, T., 2012. Axonal fiber terminations concentrate on gyri. *Cereb. Cortex* 22 (12), 2831–2839 (New York, N.Y.: 1991).
- Polimeni, J.R., Fischl, B., Greve, D.N., Wald, LL., 2010. Laminar analysis of 7T BOLD using an imposed spatial activation pattern in human. *NeuroImage* 52 (4), 1334–1346. <http://dx.doi.org/10.1016/j.neuroimage.2010.05.005>.
- Porter, D.A., Heidemann, R.M., 2009. High resolution diffusion-weighted imaging using readout-segmented echo-planar imaging, parallel imaging and a two-dimensional navigator-based reacquisition. *Magn. Reson. Med.* 62 (2), 468–475. <http://dx.doi.org/10.1002/mrm.22024>.
- Richman, D.P., Stewart, R.M., Hutchinson, J.W., Caviness, V.S., 1975. Mechanical Model of Brain Convolutional Development. New York, N.Y., *Science* 189 (4196), 18–21 (Retrieved from <http://www.ncbi.nlm.nih.gov/pubmed/1135626>).
- Ronan, L., Voets, N., Rua, C., Alexander-Bloch, A., Hough, M., Mackay, C., Fletcher, P.C., 2013. Differential tangential expansion as a mechanism for cortical gyration. *Cereb. Cortex* <http://dx.doi.org/10.1093/cercor/bht082> (New York, N.Y.: 1991).
- Sereno, M.I., Lutti, A., Weiskopf, N., Dick, F., 2013. Mapping the human cortical surface by combining quantitative T1(1) with retinotopy. *Cereb. Cortex* 23 (9), 2261–2268. <http://dx.doi.org/10.1093/cercor/bhs213> (New York, N.Y.: 1991).
- Van Essen, D.C., 1997. A tension-based theory of morphogenesis and compact wiring in the central nervous system. *Nature* 385 (6614), 313–318. <http://dx.doi.org/10.1038/38513a0>.
- Visser, E., Poser, B.A., Barth, M., Zwiers, M.P., 2012. Reference-free unwarping of EPI data using dynamic off-resonance correction with multiecho acquisition (DOCMA). *Magn. Reson. Med.* 68 (4), 1247–1254. <http://dx.doi.org/10.1002/mrm.24119>.
- Waehnert, M.D., Dinse, J., Weiss, M., Streicher, M.N., Waehnert, P., Geyer, S., Bazin, P.-L., 2013. Anatomically motivated modeling of cortical laminae. *NeuroImage* <http://dx.doi.org/10.1016/j.neuroimage.2013.03.078>.
- Xu, G., Knutsen, A.K., Dikranian, K., Kroenke, C.D., Bayly, P.V., Taber, L.A., 2010. Axons pull on the brain, but tension does not drive cortical folding. *J. Biomech. Eng.* 132 (7), 071013. <http://dx.doi.org/10.1115/1.4001683>.